

1 **Elastic anisotropy and yield surface**
2 **estimates of polycrystals**

3 R. Brenner ^{a,1} R. A. Lebensohn ^b O. Castelnau ^a

4 ^a*Laboratoire des Propriétés Mécaniques et Thermodynamiques des Matériaux,*
5 *CNRS-UPR9001, Institut Galilée, Université Paris Nord,*
6 *av. J.B. Clément, 93430 Villetaneuse, France*

7 ^b*Materials Science and Technology Division,*
8 *Los Alamos National Laboratory, Los Alamos, NM 87845, USA*

9 **Abstract**

10 Homogenization estimates based on the self-consistent scheme are customarily used
11 to describe the plastic yielding of polycrystals. Such estimates of the initial micro
12 yield surface of a polycrystal depend on the morphologic and crystallographic tex-
13 tures, the slip system geometry, the corresponding critical resolved shear stresses
14 and the single crystal elastic anisotropy. The usual approach relies on a rather crude
15 description of the stress field induced by the local elastic anisotropy. This deficiency
16 is addressed and a new concept, i.e. a “probability” yield surface is proposed. Based
17 on a statistical description of the local fields, the latter makes use of the average
18 and the standard deviation of the resolved shear stress on the different slip systems
19 within a given crystalline orientation. By comparing the homogenization estimates
20 with full-field results, it is shown that the self-consistent scheme does not present
21 intrinsic shortcomings regarding the prediction of the micro yield stress of poly-
22 crystals with anisotropic elastic constitutive behaviour. On the contrary, it delivers
23 realistic estimates if the local field fluctuations are taken into account in the yield
24 criterion. The quantitative results obtained for cubic elasticity show a strong in-
25 fluence of the intragranular stress heterogeneity on the estimate of the micro-yield
26 stress.

27 *Key words:* yield surface, polycrystals, self-consistent model, elastic anisotropy

Email address: rb@galilee.univ-paris13.fr (R. Brenner).

¹ Corresponding author

29 The initial yield surface of polycrystals can be defined in various ways. By
30 using an experimental macroscopic stress-strain curve, the *macro yield* stress
31 of a polycrystalline metallic material is customarily determined by considering
32 the stress for an offset plastic strain of 0.2%. It is assumed that all grains have
33 entered the plastic regime when this stress is reached. This conventional def-
34 inition gives necessarily an upper limit for the yield stress of the polycrystal.
35 By contrast, the *micro yield* stress corresponds to the onset of plastic slip in
36 the polycrystal. The influence of the spatial heterogeneity of elastic properties
37 on the inception of plasticity has been first brought to light qualitatively by
38 slip trace analysis in bicrystals (Hook and Hirth, 1967) and in polycrystals
39 (Hashimoto and Margolin, 1983a). Indeed, these works have reported operat-
40 ing slip systems with low Schmid factors and a preferential slip activity near
41 grain boundaries during the first stage of the elastoplastic transition. As a
42 consequence, an accurate determination of the yield stress of a polycrystal
43 requires the knowledge of the stress field that develops in the material during
44 the linear elastic regime. It should be also noted that the stress field that de-
45 velops due to elastic interaction between grains has been put forward by some
46 authors to describe the grain size dependence of the yield stress (Meyers and
47 Ashworth, 1982; Margolin et al., 1986). From an experimental point of view,
48 the recent development of microdiffraction techniques allows a quantitative
49 investigation of the crystalline lattice distortions at the grain scale (Tamura
50 et al., 2003). This technique can thus be used to detect the onset of plasticity
51 and, more generally, to characterize the local plastic response of polycrystals
52 (Castelnau et al., 2006b; Ungár et al., 2007). Such experimental results can be
53 compared with estimates derived from micromechanical modelling approaches
54 that describe the heterogeneity of the mechanical fields resulting from the mi-
55 crostructural topology and the anisotropy of the local constitutive behaviour.
56 To be more precise, micromechanical estimates of the micro yield stress are
57 functions of the spatial arrangement of grains, the crystallographic texture,
58 the slip system geometry together with the critical resolved shear stresses, and
59 the single crystal elastic moduli. To tackle this problem, two types of microme-
60 chanical approaches can be chosen: a *mean-field* modelling (i.e homogenization
61 theory) which makes use of a statistical description of the microstructure and
62 a *full-field* computation based on a spatial description of the microstructure.

63 The link between the single crystal elastic anisotropy and the onset of yielding
64 in polycrystals has been first studied within the homogenization framework by
65 Hutchinson (1970) who used the linear elastic self-consistent model (Hershey,
66 1954; Kröner, 1958) to estimate the micro yield stress. Hutchinson defined
67 the latter as the lowest macroscopic stress required to activate plastic slip
68 within the polycrystal. His self-consistent analysis relied on the average stress
69 field at the grain scale determined by using the Eshelby's inclusion result

70 (Eshelby, 1957). Since then, this model has been widely used to simulate ex-
71 periments (see, for instance, Turner et al., 1995; Clausen et al., 1998; Pang
72 et al., 1999). However, Hutchinson reported that the self-consistent model de-
73 scribes an increase of the plastic yielding onset compared to the isotropic elas-
74 tic case, whereas elastic heterogeneities are expected to decrease the initial
75 yield point. This feature has been interpreted as a shortcoming of the self-
76 consistent model which was mistakenly believed to deliver an homogeneous
77 stress field within each grain of the polycrystal. Indeed, Hutchinson explained
78 this apparent drawback by stating that "... The reason for this stems from
79 the fact that stresses in each grain are calculated by treating it as a spherical
80 inclusion. Stresses in the matrix surrounding the inclusion do not enter into
81 the self-consistent estimate of initial yield ... " (Hutchinson, 1970). With this
82 remark in mind, one of the purposes of the present paper is to derive new
83 self-consistent estimates of the micro yield stress by making use of the entire
84 available information on the stress fluctuations within the polycrystalline ma-
85 terial. To this end, comparisons with corresponding full-field solutions will be
86 instrumental to validate our homogenization analysis.

87 Numerous works have been devoted to the full-field modeling of the elastic
88 response of locally anisotropic polycrystalline aggregates, in connection with
89 the microplasticity onset. The Finite Element Method (FEM) has been cus-
90 tomarily chosen to perform this analysis. Among others, we can cite the early
91 study of Hashimoto and Margolin (1983b) on polycrystalline α -brass with
92 columnar grains, the work of Kumar et al. (1996) who considered a three-
93 dimensional (3-D) Poisson-Voronoi tessellation, and the recent investigations
94 on thin films microstructures (Wikström and Nygards, 2002; Geandier et al.,
95 2008) and fields distribution at free surfaces (Sauzay, 2007; Zeghadi et al.,
96 2007). These different studies clearly evidenced the influence of the elastic
97 heterogeneities on the stress field fluctuations, especially near grain bound-
98 aries. It is clear that, beyond the description of the effective behaviour, full-
99 field models provide significant information on local fields. They can thus be
100 used to characterize the local fields distribution and to assess the accuracy
101 of homogenization estimates at *both* macroscopic and local scales. Such com-
102 parisons have been performed for viscoplastic polycrystals (Lebensohn et al.,
103 2004), by using a method based on Fast Fourier Transform (FFT) (Moulinec
104 and Suquet, 1998; Lebensohn, 2001), but few detailed studies exist for pol-
105 crystal elasticity. This question has been only partially addressed by Yaguchi
106 and Busso (2005) who performed comparisons of the overall elastic properties
107 of columnar microstructures.

108 In this paper, we first present a thorough analysis of the local fields distribution
109 within a Representative Volume Element (RVE) of an elastic polycrystalline
110 aggregate using, on the one hand, the FFT-based full-field modelling and, on
111 the other hand, the self-consistent scheme (Section 2). Next, the link between
112 the elastic stress field and the definition of the micro yield stress, which con-

stitutes the central issue of this article, is discussed and an original probability approach for the determination of the yield surface is described (Section 3). Using this “probability” yield surface, the accuracy of various self-consistent estimates, including the one given by Hutchinson (1970), is then discussed by comparison with reference full-field results (Section 4).

2 Local fields within elastic polycrystals

Let us consider a RVE with volume Ω of an elastic polycrystalline medium. In what follows, the notion of *representativity* encompasses both mechanical and microstructural definitions. Thus, the volume Ω is said representative if: (i) Hill’s macrohomogeneity condition is fulfilled and (ii) all the statistical information on the microstructure is contained in Ω (Hill, 1963). Our study is concerned with polycrystals presenting a random homogeneous and isotropic microstructure. This implies, in particular, equiaxed grains and a random repartition of the crystalline orientations within the material. Besides, it is assumed that the elastic tensor field $\mathbf{C}(\mathbf{x})$ is ergodic. It is worth noting that the RVE status of such random media has been rigorously justified (Sab, 1992).

2.1 Full-field modelling: FFT-based method

Given a complete description of a polycrystalline microstructure, various numerical methods can be used to compute its mechanical response. Up to now, the FEM remains the most widely used. In this article, we chose to use an alternative method, originally proposed by Moulinec and Suquet (1998), which makes use of the Fourier transform technique to solve the heterogeneous elasticity problem in a periodic unit cell. This method relies on the integral equation for the strain field, also called Lippmann-Schwinger equation (see, for instance, Zeller and Dederichs, 1973). The main attracting features of this numerical scheme are the possibility of using images of the microstructure as direct input (no meshing required) and a low numerical cost (problems with several millions of degrees of freedom (d.o.f.) can be solved in a few minutes without parallel computing, see Appendix B). The reader is referred to Moulinec and Suquet (1998); Eyre and Milton (1999); Michel et al. (2001) for a detailed description of the method and to Lebensohn (2001) who first used it to investigate the local response of elastic and viscoplastic polycrystalline aggregates made of cubic-shaped grains.

146 *2.1.1 Unit cell description*

147 To construct a cubic polycrystalline unit cell of volume Ω_{UC} , a Poisson-Voronoi
 148 tessellation has been chosen. Dating from the work of Kumar and Kurtz (1994),
 149 this microstructural model is widely used to study the physical properties of
 150 equiaxed polycrystalline microstructures because it mimics the homogeneous
 151 crystal growth process. Note that in our case periodicity has to be imposed on
 152 the microstructure to be consistent with the requirements of the FFT-based
 153 method and to avoid artificial boundary effects (see also Nygard and Gud-
 154 mundson, 2002). This is ensured by the periodic duplication of Voronoi seeds
 155 immediately outside the unit cube. A set of 500 initial seeds is used to gen-
 156 erate the tessellation and a uniform crystalline orientation is assigned to each
 157 resulting Voronoi cell. For that goal, a set \mathcal{N}_φ of 500 crystalline orientations
 158 generated with a quasi-random Sobol process has been used. There is thus
 159 a one-to-one correspondence between the set of Voronoi cells and the set of
 160 crystalline orientations. The obtained cubic unit cell is further discretized into
 161 a regular grid consisting of $128 \times 128 \times 128$ voxels (Figure 1a). Each grain thus
 162 comprises 4,200 voxels on average. The set of orientations \mathcal{N}_φ and the Voronoi
 163 tessellation process lead to a quasi-isotropic Orientation Distribution Function
 164 (ODF). Consequently, the volumetric average of the elastic tensor field over an
 165 unique unit cell is quasi-isotropic and can be considered as a good approxima-
 166 tion of its ensemble average (i.e. 1-point correlation function) over the set of
 167 equiprobable realizations \mathcal{P}_α . It can thus be concluded that a polycrystalline
 168 unit-cell of volume Ω_{UC} is isotropic of grade 1 following Kröner’s terminology
 169 (Kröner, 1977). By contrast, for grade $n > 1$, the volumetric average over Ω_{UC}
 170 does not *a priori* identify with the n -point correlation function and it follows
 171 that the ergodicity assumption is not verified by Ω_{UC} . Consequently, the con-
 172 structed unit cell *is not* a RVE. In particular, it does not contain several grains
 173 with the same crystalline orientation but different neighbouring environments.

174 *2.1.2 Approximation of the RVE’s response*

To approximate the RVE’s response of a polycrystal, we apply the procedure
 of ensemble averaging (see, for instance, Sab, 1992). Let α be a particular
 realization in the set \mathcal{P}_α of equiprobable realizations (i.e. the set of cubic unit
 cells generated by Poisson-Voronoi tessellation) and let t be a random field,
 statistically homogeneous and ergodic. Then, the expectation of t defined by
 $\langle t \rangle^{\mathcal{P}_\alpha} = \int_{\mathcal{P}_\alpha} t(\alpha) d\alpha$ can be approximated by a Monte-Carlo computation

$$\langle t \rangle^{\mathcal{P}_\alpha} \approx \frac{1}{N_\alpha} \sum_{i=1}^{N_\alpha} t(\alpha_i) \quad (1)$$

175 with N_α being the number of unit cell realizations. The ergodicity assumption
 176 implies that the expectation of t is equal to the volumic average of t over Ω .

177 Note that the generation of different unit cells is performed with the fixed set
 178 of orientations \mathcal{N}_φ and randomly varying Voronoi seeds positions. Grains with
 179 the same crystalline orientation but varying neighbourhoods are thus present
 180 in the different realizations. This allows us to also perform rigorous ensemble
 181 averages of the mechanical fields per crystalline orientation.

182 2.1.3 Fields description

183 An important aspect of the present analysis is to assess the accuracy of the
 184 ensemble averaging procedure at different scales. In order to perform ensemble
 185 averages, we have generated 100 unit cell realizations and considered the local
 186 constitutive elastic behaviour of a crystal with cubic lattice symmetry. The
 187 anisotropy of the local elastic behaviour can be characterized by the parame-
 188 ter A introduced by Zener (1948), which reads, using standard Voigt notation:
 189 $A = 2C_{44}/(C_{11} - C_{12})$. Each unit cell has been subjected to uniaxial tensile,
 190 simple shear and mixed tensile-shear loadings. For illustration, the axial stress
 191 field distribution, normalized by the corresponding macroscopic value, for a
 192 tensile loading and anisotropy parameter $A = 2.8$ is shown in Figure 1b. As ex-
 193 pected, strong fluctuations of the local axial stress are obtained, with maxima
 194 appearing preferentially close to grain boundaries and a stress concentration
 195 factor varying between 0.4 and 1.6 for this particular unit cell.

While some results have been reported in the literature on the size of the
 RVE necessary to estimate the effective properties of polycrystalline materials
 within a given error (see, e.g. Nygard, 2003; Houdaigui et al., 2007), in the
 present investigation we analyze the representativity of our results at both
 macroscopic and local scales (“local” refers here to the scale of individual
 crystals). According to sampling theory, the relative error on the expectation
 of an homogeneous and ergodic random variable t is expressed as

$$\epsilon_t = \frac{2 \text{SD}^{\mathcal{P}_\alpha}(t)}{\langle t \rangle^{\mathcal{P}_\alpha} \sqrt{N_\alpha}} \quad (2)$$

196 where the standard deviation $\text{SD}^{\mathcal{P}_\alpha}(t)$ and the average $\langle t \rangle^{\mathcal{P}_\alpha}$ are approximated
 197 by a Monte-Carlo computation of the ensemble average on N_α realizations
 198 (1). The error ϵ_t is thus important when the random variable t strongly vary
 199 from one realization to another. To quantify the accuracy of the full-field
 200 results at different scales, we have considered three random variables: the
 201 overall equivalent stress $\bar{\sigma}_{\text{eq}}$, the equivalent of the average stress $\langle \sigma \rangle_{\text{eq}}^r$ and
 202 the standard deviation of the equivalent stress $\text{SD}^r(\sigma_{\text{eq}})$ within a given grain
 203 orientation which has been arbitrarily chosen in the set \mathcal{N}_φ . The evolution of
 204 the sampling error for each variable with respect to the number of realizations
 205 N_α is reported on Figure 2, for Zener parameter $A = 2.8$, in the case of a
 206 tensile loading. As expected, a decrease of the error ϵ is obtained with the

207 increase of \mathcal{N}_α . It is worth mentioning that the minimum attainable error
 208 depends on the local anisotropy, the discretization and the size of the unit
 209 cell. In the studied case, we obtain a relative error of 0.1% on the macroscopic
 210 stress, 1% on the average stress per grain orientation and 5% on the standard
 211 deviation of the stress within a grain orientation for 100 realizations. There
 212 is thus one to two orders of magnitude between the precisions at the overall
 213 and local scales for the chosen local description of the stress field. This result
 214 can be explained by the fact that the overall stress depends at first order
 215 on the 1-point correlation function of the elastic tensor field which slightly
 216 varies from one realization to another. By contrast, the average and standard
 217 deviation of the local stress within a grain with a given crystalline orientation
 218 is strongly affected by its neighbourhood (i.e. by higher-order correlation
 219 functions of the elastic tensor field). This results in less accurate estimates
 220 of the local fields compared to the macroscopic fields, for a given number of
 221 realizations. The effect of the neighbouring grains on the local stress field can
 222 be further illustrated by investigating the stress distributions. Figure 3 shows
 223 the effect of the number of realizations on the shape of the distribution within
 224 a given crystalline orientation. For a single realization, the stress distribution
 225 within a single crystalline orientation is far from Gaussian, but it gets closer
 226 to Gaussian when many random realizations are considered although there
 227 is no proof that it becomes really Gaussian. The addition of different grain
 228 environments thus tends to smooth out the local stress field distribution. It is
 229 emphasized that this distribution is expected to be a good approximation of
 230 the one that would have been obtained if we had considered a polycrystalline
 231 volume element containing grains with the same crystalline orientation but
 232 randomly located in the specimen as in Castelnau et al. (2006a). On the
 233 other hand, it can be observed that the stress field distribution in the whole
 234 sample is already almost symmetric for a single unit cell (Figure 3). It should
 235 be mentioned that field distributions close to Gaussian have previously been
 236 reported in two-dimensional linear composites with “particulate” (i.e. matrix–
 237 inclusion) microstructure (Moulinec and Suquet, 2003).

238 2.2 Mean-field modelling: Self-consistent scheme

By contrast with the previous full-field numerical approach, mean-field esti-
 mates (a.k.a homogenization estimates) rely on an incomplete statistical de-
 scription of the microstructure. In the case of polycrystals, the heterogeneity
 is related to the existence of different crystalline orientations or *mechanical*
phases. Each mechanical phase r has a volume Ω_r , and its spatial repartition
 is described by the characteristic function $\chi^r(\mathbf{x})$, which is equal to 1 if $\mathbf{x} \in \Omega_r$
 and 0 otherwise. An elastic polycrystal can be considered to be a composite

material made of N crystalline orientations such that

$$\mathbf{C}(\mathbf{x}) = \sum_{r=1}^N \mathbf{C}^r \chi^r(\mathbf{x}) \quad (3)$$

239 where \mathbf{C}^r is the elastic moduli tensor of mechanical phase r . The microstruc-
 240 ture of the polycrystalline material is statistically described by the n -point
 241 correlation functions of the characteristic functions. Due to the “granular”
 242 character of a polycrystal (i.e. all crystalline orientations are on the same foot-
 243 ing), the self-consistent model (Hershey, 1954) is expected to be well adapted
 244 for this kind of microstructures (see Kröner, 1978). It is recalled that, in a
 245 homogenization context, the localization problem linking the local strain field
 246 $\boldsymbol{\varepsilon}(\mathbf{x})$ to the overall strain $\bar{\boldsymbol{\varepsilon}}$ cannot be solved. Nevertheless, using the statisti-
 247 cal description of the microstructure and the uniformity per phase of the local
 248 behaviour, the problem can be degenerated by considering only the average
 249 localization for each crystalline orientation.

250 2.2.1 Self-consistent estimate

By considering ellipsoidal 2-point correlation functions (Willis, 1977), the es-
 timate of the effective elastic tensor $\tilde{\mathbf{C}}$ can be derived using Eshelby’s solution
 (Eshelby, 1957) for an ellipsoidal inclusion embedded in an infinite homoge-
 neous linear medium, itself subjected to an homogeneous loading. The self-
 consistent estimate of $\tilde{\mathbf{C}}$ reads

$$(\tilde{\mathbf{C}} + \mathbf{C}^*)^{-1} = \langle (\mathbf{C} + \mathbf{C}^*)^{-1} \rangle \quad (4)$$

251 where $\mathbf{C}^* = \mathbf{P}^{-1} - \tilde{\mathbf{C}}$ is the “constraint” tensor which reflects the reaction of
 252 the homogeneous medium to the deformation of the inclusion. It depends on
 253 the Hill tensor \mathbf{P} which is a function of the elastic properties of the effective
 254 medium and the shape of the inclusion (see Appendix A).

At the local scale, the self-consistent model delivers information about the
 average fields per crystalline orientation. For instance, the local average strain
 tensor reads

$$\langle \boldsymbol{\varepsilon} \rangle^r = (\mathbf{C}^r + \mathbf{C}^*)^{-1} : (\tilde{\mathbf{C}} + \mathbf{C}^*) : \bar{\boldsymbol{\varepsilon}} \quad (5)$$

The local average stress tensor can be obtained using the constitutive relation:
 $\langle \boldsymbol{\sigma} \rangle^r = \mathbf{C}^r : \langle \boldsymbol{\varepsilon} \rangle^r$. However, the statistical description of the local stress and
 strain fields is not limited in the mean-field framework to this first-order infor-
 mation. Indeed, the homogenization procedure also delivers estimates of the
 field fluctuations. More precisely, the second moment of the intraphase field
 distribution can be obtained by considering partial derivatives of the effective
 elastic energy with respect to the local elastic behaviour (see Bergman, 1978;
 Bobeth and Diener, 1987; Kreher, 1990; Ponte Castañeda and Suquet, 1998).

This result follows from the quadratic dependence of the elastic energy on the stress and strain fields. For instance, the intraphase second moment of the strain field for crystalline orientation r is given by

$$\langle \boldsymbol{\varepsilon} \otimes \boldsymbol{\varepsilon} \rangle_{ijkl}^r = \frac{1}{c_r} \bar{\boldsymbol{\varepsilon}} : \frac{\partial \tilde{\mathbf{C}}}{\partial C_{ijkl}^r} : \bar{\boldsymbol{\varepsilon}}. \quad (6)$$

255 Its explicit computation, in a general anisotropy context, is given in Appendix
256 A.

257 2.2.2 Fields description

258 The self-consistent estimate of the elastic response of the polycrystalline RVE
259 has been computed numerically. In doing this, we have considered a spherical
260 shape for the covariances and the above-described set \mathcal{N}_φ of crystalline orien-
261 tations with equal weights. The implicit self-consistent equation (4) has been
262 solved iteratively with a relative error of 10^{-6} . The good agreement between
263 the FFT-based computations and the linear self-consistent estimate has been
264 previously reported for different polycrystalline microstructures, namely: 2-D
265 Voronoi tessellations (Castelnau et al., 2006a) and 3-D polycrystals with cubic
266 grains (Lebensohn et al., 2004), and was expected to also hold in the present
267 3-D Voronoi case. Indeed, a relative error of about 1% is obtained on the av-
268 erage and second moment of the stress and strain distributions within each
269 crystalline orientation. This is the minimum error that could be achieved since
270 it is of the same order as the sampling error on the intragranular average and
271 standard deviation of the stress field, as already discussed (Figure 2).

272 3 Yield surface estimates

273 The results of the previous section highlight the strong stress heterogeneity
274 induced in a polycrystalline RVE made of grains with local elastic anisotropy.
275 Moreover, the pertinence of the self-consistent scheme to describe the stress
276 field distribution for linear polycrystal has been demonstrated by comparison
277 with full-field computations. Based on these results, the way in which this
278 available statistical information can be used to accurately describe the onset
279 of plasticity in a polycrystal is now addressed.

280 3.1 Shortcoming of previous mean-field estimates

As discussed previously, Hutchinson (1970) was the first to shed light on the influence of the local elastic anisotropy on the micro yield stress estimated

by means of the self-consistent scheme. Indeed, earlier assessments of the self-consistent model for elastoplastic polycrystals relied on a simplifying assumption of elastic isotropy (Budiansky et al., 1960; Kröner, 1961). Hutchinson's analysis focused on the self-consistent prediction of the initial yield surface of a random polycrystal made of FCC single crystals. For this crystalline symmetry, the slip set \mathcal{K} comprises 12 crystallographically equivalent slip systems $\{111\}[1\bar{1}0]$. By adopting a description of the local stress field limited to its intraphase mean values, he showed that the self-consistent scheme leads to a modified Tresca criterion, with a yield function f_Y of the form

$$f_Y(\bar{\boldsymbol{\sigma}}) = \max_{I,J} \frac{|\bar{\sigma}_I - \bar{\sigma}_J|}{2} - \tilde{\tau}_0 \quad (7)$$

where σ_I ($I = 1, 2, 3$) are the macroscopic principal stresses. The effective yield stress $\tilde{\tau}_0$ is given by (Hutchinson, 1970)

$$\tilde{\tau}_0 = \tau_0 \sqrt{\frac{3}{2a^2 + b^2}} \quad (8)$$

where the coefficients a and b are

$$a = \frac{C_{11} - C_{12}}{2\tilde{\mu}(1 - \beta) + \beta(C_{11} - C_{12})}, \quad b = \frac{C_{44}}{\tilde{\mu}(1 - \beta) + \beta C_{44}}, \quad \beta = \frac{6}{5} \left(\frac{\tilde{\kappa} + 2\tilde{\mu}}{3\tilde{\kappa} + 4\tilde{\mu}} \right) \quad (9)$$

with $\tilde{\kappa}$ and $\tilde{\mu}$ being the self-consistent estimates of the effective bulk and shear moduli. For cubic polycrystals, it is well-known that the effective bulk modulus coincides with the bulk modulus of the crystallites (Hill, 1952; Mendelson, 1981) whereas the self-consistent overall shear modulus is the positive root of the following cubic equation (Hershey, 1954; Kröner, 1958)

$$8\tilde{\mu}^3 + (5C_{11} + 4C_{12})\tilde{\mu}^2 - C_{44}(7C_{11} - 4C_{12})\tilde{\mu} - C_{44}(C_{11} - C_{12})(C_{11} + 2C_{12}) = 0. \quad (10)$$

281 For an isotropic local elastic behaviour (i.e leading to an uniform stress field
 282 within the polycrystal), relation (8) gives $\tilde{\tau}_0 = \tau_0$ so that the yield function
 283 (7) reduces to the Tresca yield surface (Hill, 1967).

284 To highlight the influence of the elastic anisotropy on the stress heterogene-
 285 ity, we have considered different values of the Zener anisotropy parameter.
 286 The equivalent stress distribution within the RVE for a tensile loading are
 287 reported on Figure 4. In the case $A = 1$ (i.e elastic isotropy), the distribution
 288 is a Dirac delta function since the polycrystal is homogeneous. An increase
 289 of the local anisotropy leads to a spread and a shift of the peak to larger
 290 stress values. Similar observations have been made previously in a nonlinear
 291 context for viscoplastic polycrystals with highly anisotropic grains (see, for
 292 instance, Castelnau et al., 2008). Figure 4 illustrates that an increase of the
 293 local anisotropy implies an increase of the stress heterogeneity, which in turn
 294 should induce an early plastic yielding of the polycrystal, compared to the

295 isotropic elasticity case (i.e. Tresca yield surface). On the contrary, Hutchin-
 296 son (1970) observed that the expression of the effective yield stress (equation
 297 8) predicts a delayed plastic yielding for a Zener elastic anisotropy parameter
 298 A greater than 1 (which is the case of many common metals: Cu, Fe, Al, Ni
 299 ...). Up to now, this apparent deficiency of the self-consistent model has not
 300 been addressed.

301 3.2 New statistical yield criterion incorporating field fluctuations

In order to improve the self-consistent estimate of yielding, we propose to take into account the available information on local stress fluctuations. First, we consider a RVE for which the microstructure is perfectly known. The local Resolved Shear Stress (RSS) on a slip system k , at a given point \mathbf{x}^g of the grid, can be obtained as

$$\tau_k(\mathbf{x}^g) = \boldsymbol{\sigma}(\mathbf{x}^g) : \sum_{r=1}^N \boldsymbol{\mu}_k^r \chi^r(\mathbf{x}^g) \quad (11)$$

where $\boldsymbol{\mu}_k^r$ is the Schmid tensor of slip system k within crystalline orientation r . According to the Schmid criterion, plasticity occurs when the following condition is fulfilled

$$\max_{\mathbf{x}^g \in \Omega} \max_{k \in \mathcal{K}} |\tau_k(\mathbf{x}^g)| = \tau_0. \quad (12)$$

302 Although it appears to be a quite straightforward approach to describe the
 303 micro-yield stress of the polycrystal, this definition presents some important
 304 drawbacks. Indeed, it is dependent on the refinement of the grid used for the
 305 full-field numerical resolution and, because of the random character of the
 306 microstructure, it leads to a yield stress estimate that strongly vary from one
 307 unit cell to another. This prevents the use of this criterion to get an accurate
 308 estimate of the onset of plasticity.

An alternative approach to define the micro-yield stress is making use of the field statistics information. Obviously, different estimates of the onset of plasticity can be obtained, depending on the order of the statistical parameters involved in the yield criterion. For example, Hutchinson (1970) made a very specific choice, disregarding the intraphase stress heterogeneity, defining that yielding of the polycrystal occurs when

$$\max_{r \in \mathcal{N}_\varphi} \max_{k \in \mathcal{K}} |\langle \tau_k \rangle^r| = \tau_0 \quad (13)$$

where \mathcal{N}_φ is the finite set of crystalline orientations chosen to represent the crystallographic texture of the polycrystal and $\langle \tau_k \rangle^r = \boldsymbol{\mu}_k^r : \langle \boldsymbol{\sigma} \rangle^r$. We propose

a more flexible and general definition of the plastic onset that reads

$$\max_{r \in \mathcal{N}_\varphi} \max_{k \in \mathcal{K}} \hat{\tau}_k^r = \tau_0 \quad (14)$$

where $\hat{\tau}_k^r$ is a Reference Resolved Shear Stress (RRSS) that needs to be specified in the general case of a nonuniform intraphase stress field. Based on the information on the local fields that can be obtained with homogenization theory, we propose the following expression

$$\hat{\tau}_k^r = |\langle \tau_k \rangle^r| + p \text{SD}^r(\tau_k) \quad (15)$$

which involves the mean value $\langle \tau_k \rangle^r$ and the standard deviation $\text{SD}^r(\tau_k)$ of the RSS on slip system k of crystalline orientation r . The latter is given by

$$\text{SD}^r(\tau_k) = \sqrt{\langle \tau_k^2 \rangle^r - (\langle \tau_k \rangle^r)^2} \quad \text{with} \quad \langle \tau_k^2 \rangle^r = \boldsymbol{\mu}_k^r : \langle \boldsymbol{\sigma} \otimes \boldsymbol{\sigma} \rangle^r : \boldsymbol{\mu}_k^r. \quad (16)$$

309 Depending on the value of the positive parameter p , relation (15) leads to dif-
 310 ferent estimates of the initial yield stress of the polycrystal. These estimates
 311 can be evaluated for different applied loadings by using the self-consistent
 312 scheme or the full-field numerical scheme to determine a so-called *probability*
 313 *yield surface*. This terminology has been chosen by analogy with the notion
 314 of confidence intervals in Statistics, which indicate the probability of a mea-
 315 surement falling within p standard deviations of the mean (e.g. for a Gaussian
 316 distribution, this probability is equal to 0.683 for $p = 1$ and 0.997 for $p = 3$).
 317 In the present context, this probability is related to the stress heterogene-
 318 ity accounted for by the new yield criterion. The value of p parameter can
 319 also be related to a more intuitive quantity, i.e. a threshold volume fraction
 320 of the grain where plasticity initiates that needs to be in yielding condition
 321 to consider that the polycrystal is at the onset of plasticity. This threshold
 322 volume fraction decreases as p increases (e.g. if the field distributions in the
 323 grains are strictly Gaussians, $p = 1$ amounts to consider that 15.85% of the
 324 first plastifying grain has to yield, while for $p = 3$ only a tiny 0.15% volume
 325 fraction has to be deforming plastically, to consider that the polycrystal has
 326 reached the plasticity onset. Note that the previous estimate of Hutchinson
 327 (1970) corresponds to a threshold volume fraction of 50%).

328 4 Results and discussion

329 The probability yield criterion (14) and (15) is now applied to the class of
 330 polycrystals discussed in Section 2 and its main features are compared to
 331 previous works.

332 First, the accuracy of our self-consistent estimates have been assessed by con-
 333 frontation with the FFT results. For that goal, sections of the yield surface in

334 the “tension-torsion” plane have been computed, for several assumed p val-
 335 ues, using expression (15). Self-consistent calculations were performed with 5°
 336 steps while FFT computations were carried out for three particular loading
 337 directions: uniaxial tension, pure torsion and a mixed “tension-torsion” load-
 338 ing (Figure 5) (In the case $p = 0$, the self-consistent numerical computations
 339 have been also compared with the analytic solution (8), showing a very good
 340 agreement, with a relative discrepancy of about 10^{-3} , likely to be linked to the
 341 finite set of crystalline orientations used to approximate an isotropic crystallo-
 342 graphic texture). A very good agreement is obtained between the FFT-based
 343 and the self-consistent yield surfaces, for any p value. This is a direct conse-
 344 quence of the excellent agreement between first and second moments of the
 345 field distributions within different crystalline orientations computed with both
 346 approaches. An important conclusion is thus that the self-consistent model
 347 does not present intrinsic drawback concerning the description of the micro-
 348 yield stress. The shortcoming of Hutchinson’s estimate appears to be uniquely
 349 related to the choice of the RRSS in the yield criterion (i.e. $\hat{\tau}_k^r = \langle \tau_k \rangle^r$). It is
 350 observed that earlier plastic onsets can be predicted when stress heterogene-
 351 ity enters the yield criterion ($p > 0$). Note also that the yield surfaces remain
 352 convex for any p value.

353 Second, we investigated the physical relevance of the new estimates by com-
 354 puting the evolution of the tensile yield stress for various Zener anisotropy
 355 parameters A . In Figure 6, results are reported for different p values as well as
 356 the Tresca yield stress ($\sigma_Y/\tau_0 = 2$). Drastically different variations of the yield
 357 stress with the local anisotropy are obtained. For $p = 0$, the self-consistent
 358 scheme predicts an increase of the yield stress with respect to the isotropic
 359 elastic case, for whatever value of the Zener parameter. This result is in strong
 360 disagreement with the stress fluctuations that develop in the polycrystal when
 361 the local anisotropy increases (Figure 4). By contrast, when the intragranular
 362 stress heterogeneity is used to define the RRSS ($p > 0$), the yield stress re-
 363 mains below the Tresca limit and decreases monotonically when A increases.
 364 Such behavior is consistent with an increasing heterogeneity as anisotropy
 365 increases.

366 In what follows, the influence of the field heterogeneity on the shape of the
 367 yield criterion is addressed. A section of the yield surface in the $(\tilde{\sigma}_{11}, \tilde{\sigma}_{22})$ plane
 368 is reported in Figure 7 for two values of the Zener parameter. When $p = 0$,
 369 Hutchinson (1970) showed that the “classical” self-consistent scheme deter-
 370 mines a *modified* Tresca condition, i.e the yield surface is obtained by dilation
 371 of the Tresca yield surface and thus remains a hexagon in such projection.
 372 When the stress heterogeneity is considered in the yield criterion, this is no
 373 longer the case. Indeed, our results show that the yield surface departs from a
 374 Tresca-type condition. It can be observed that the initially straight segments
 375 of the yield surface become curved when stress fluctuations are considered.
 376 This deviation from the Tresca-type yield surface is more pronounced for in-

377 creasing values of parameters A and p . These results indicate that, in general,
378 the initial yield surface of macroscopically isotropic elastoplastic polycrystals
379 does not obey a Tresca-type criterion (7).

380 5 Concluding remarks

381 This study sheds light on the effects of the local elastic anisotropy on the onset
382 of plasticity of polycrystalline materials. Our attention has been focused on
383 the description of yielding that can be obtained by means of homogenization
384 theories. Based on a statistical description of local fields and the Schmid cri-
385 terion, it has been shown that there is not an unique definition of the initial
386 yielding of elastoplastic polycrystals, unless elasticity is isotropic. The defini-
387 tion based on the absolute maximum resolved shear stress in the RVE is useless
388 since this extreme value cannot be determined, except maybe for very specific
389 microstructures for which the complete stress field can be solved analytically.
390 We have proposed an original definition of the initial yield criterion based
391 on field statistics. This new approach defines a set of “probability” yield sur-
392 faces. These latter can be associated to threshold volume fractions of the first
393 plastic grain that needs to be in yielding condition. Addressing Hutchinson’s
394 remark on an apparent shortcoming of the self-consistent scheme, it has been
395 demonstrated that the incorporation of field fluctuations in the yield criterion
396 leads to physically meaningful self-consistent estimates. In particular, an ear-
397 lier plastic initiation compared with the elastically isotropic case is predicted
398 and a monotonic decrease of the yield stress estimate is obtained when the
399 stress fluctuations increase. The self-consistent estimates have been success-
400 fully compared with the results of full-field computations performed on 3-D
401 polycrystalline microstructures. Concerning the shape of the yield surface, our
402 investigation highlights the fact that the new “probability” yield surface does
403 not generally follow a Tresca-type criterion. A detailed investigation of the
404 relation between the field fluctuations and the shape of the yield surface, as
405 well as the extension of the present statistical approach to describe the evolu-
406 tion with strain of the yield surface will be subjects of future work. Finally, it
407 is mentioned that the proposed approach might open interesting perspectives
408 for related problems, such as twinning activation in low-symmetry crystalline
409 structures, stress-assisted phase transformation, brittle fracture criterion in
410 polycrystalline ceramics etc. In all these problems, the local stresses distribu-
411 tion plays a critical role and should be taken into account.

412 **Figure Captions**

413 Figure 1: Periodic Poisson-Voronoi tessellation containing 500 grains with uni-
414 form crystalline orientations (a) and corresponding axial stress field for a ten-
415 sile loading (b).

416 Figure 2: Relative sampling error of the stress field at different scales vs. the
417 number of unit-cell realizations.

418 Figure 3: Normalized equivalent stress field distribution within a single crys-
419 talline orientation (left) and within the whole unit-cell (right). Note that a
420 similar distribution is obtained with 100 configurations for the whole unit-
421 cell.

422 Figure 4: Distribution of the equivalent stress field distribution within a poly-
423 crystalline RVE, for different values of the Zener parameter A , as obtained by
424 the full-field approach.

425 Figure 5: Self-consistent estimates of yield surface sections obtained with dif-
426 ferent p values for tension-torsion loadings (curves). FFT estimates are re-
427 ported for three different loading paths (symbols).

428 Figure 6: Self-consistent estimates of the tensile yield stress as a function of
429 the Zener parameter A . Note that the case $p = 0$ corresponds to Hutchinson's
430 estimate. The horizontal dotted line indicates the value of the Tresca yield
431 stress.

432 Figure 7: Self-consistent estimates of yield surface sections obtained with dif-
433 ferent p values for biaxial loadings. $A = 2.8$ (left) and $A = 10$ (right).

434 Figure 8: CPU time per elastic FFT iteration as a function of the number of
435 voxels N . The white squares correspond to unit-cell discretizations with prime
436 numbers in each direction.

437 **A Computation of intraphase second moments of stress and strain**
 438 **fields**

439 The numerical computation of the intraphase stress second moment for the
 440 self-consistent model has been discussed previously in (Brenner et al., 2004). It
 441 must be noted that the expressions obtained in this article require symmetriza-
 442 tion but this had no consequences on the published results. In this appendix,
 443 we derive the concise dual expression for the intraphase strain second moment.

The intraphase stress and strain second moments are linked by the local constitutive elastic law

$$\langle \boldsymbol{\sigma} \otimes \boldsymbol{\sigma} \rangle^r = \mathbf{C}^r : \langle \boldsymbol{\varepsilon} \otimes \boldsymbol{\varepsilon} \rangle^r : \mathbf{C}^r. \quad (\text{A.1})$$

An estimate of the strain second moment can be obtained via the relation

$$\langle \boldsymbol{\varepsilon} \otimes \boldsymbol{\varepsilon} \rangle_{ijkl}^r = \frac{1}{c_r} \bar{\boldsymbol{\varepsilon}} : \frac{\partial \tilde{\mathbf{C}}}{\partial C_{ijkl}^r} : \bar{\boldsymbol{\varepsilon}} \quad (\text{A.2})$$

444 A detailed proof of the above relation can be found, in e.g. (Ponte Castañeda
 445 and Suquet, 1998).

446 *A.1 Computation of $\partial \tilde{\mathbf{C}} / \partial C_{ijkl}^r$*

The partial derivatives of the self-consistent equation (4) with respect to local elastic moduli reads

$$\tilde{\mathbf{F}} : \frac{\partial (\tilde{\mathbf{C}} + \mathbf{C}^*)}{\partial C_{ijkl}^r} : \tilde{\mathbf{F}} - \left\langle \mathbf{F} : \frac{\partial \mathbf{C}^*}{\partial C_{ijkl}^r} : \mathbf{F} \right\rangle = \left\langle \mathbf{F} : \frac{\partial \mathbf{C}}{\partial C_{ijkl}^r} : \mathbf{F} \right\rangle \quad (\text{A.3})$$

with $\tilde{\mathbf{F}} = (\tilde{\mathbf{C}} + \mathbf{C}^*)^{-1}$ and $\mathbf{F} = (\mathbf{C} + \mathbf{C}^*)^{-1}$. The latter is a linear system of equations for the determination of $\partial \tilde{\mathbf{C}} / \partial C_{ijkl}^r$. Using Kelvin's convention to represent symmetric fourth order tensors in three dimensions by symmetric second order tensors in six dimensions (Mehrabadi and Cowin, 1990), the latter equation is expressible in the form

$$\Delta_{IJKL} \frac{\partial \tilde{C}_{KL}}{\partial C_{PQ}^r} = \Phi_{IJ}^{r,PQ} \quad (\text{A.4})$$

with

$$\begin{aligned}
\Delta_{IJKL} &= \tilde{F}_{IK}\tilde{F}_{LJ} + \tilde{F}_{IM}Q_{MNKL}\tilde{F}_{NJ} - \sum_{s=1}^N c_s F_{IM}^s Q_{MNKL} F_{NJ}^s, \\
Q_{MNKL} &= -P_{MS}^{-1} \frac{\partial P_{ST}}{\partial \tilde{C}_{KL}} P_{TN}^{-1} - \delta_{MK}\delta_{NL}, \\
\Phi_{IJ}^{r,PQ} &= \frac{1}{2}(F_{IP}^r F_{QJ}^r + F_{IQ}^r F_{PJ}^r),
\end{aligned} \tag{A.5}$$

447 where uppercase indices vary between 1 and 6. The estimation of the in-
448 traphase second moment of the strain field thus requires the evaluation of the
449 Hill tensor \mathbf{P} and its derivatives $\partial \mathbf{P} / \partial \tilde{C}_{ijkl}$. In a general context of elastic
450 anisotropy, these two quantities have to be computed numerically.

451 A.2 Computation of \mathbf{P} and $\partial \mathbf{P} / \partial \tilde{C}_{ijkl}$

The Hill tensor \mathbf{P} is defined by a surface integral on the unitary sphere

$$\mathbf{P} = \frac{1}{4\pi |\mathbf{Z}|} \int_{|\boldsymbol{\xi}|=1} \boldsymbol{\Gamma}(\boldsymbol{\xi}) |\mathbf{Z}^{-1} \cdot \boldsymbol{\xi}|^{-3} dS \tag{A.6}$$

where \mathbf{Z} is a second-order tensor defining the assumed ellipsoidal shape of the two-point correlation function of each phase. The Green operator $\boldsymbol{\Gamma}(\boldsymbol{\xi})$ reads

$$\boldsymbol{\Gamma} = [\boldsymbol{\xi} \otimes \boldsymbol{\kappa}^{-1} \otimes \boldsymbol{\xi}]^{(s)} \tag{A.7}$$

452 with the acoustic (Christoffel) tensor $\boldsymbol{\kappa} = \boldsymbol{\xi} \cdot \tilde{\mathbf{C}} \cdot \boldsymbol{\xi}$. $[\]^{(s)}$ indicates the (double)
453 minor symmetrization.

The computation of partial derivatives of the Hill tensor thus requires the evaluation of

$$\frac{\partial \boldsymbol{\Gamma}}{\partial \tilde{C}_{ijkl}} = \left[\boldsymbol{\xi} \otimes \frac{\partial \boldsymbol{\kappa}^{-1}}{\partial \tilde{C}_{ijkl}} \otimes \boldsymbol{\xi} \right]^{(s)} \tag{A.8}$$

with

$$\frac{\partial \boldsymbol{\kappa}^{-1}}{\partial \tilde{C}_{ijkl}} = -\boldsymbol{\kappa}^{-1} \cdot \frac{\partial \boldsymbol{\kappa}}{\partial \tilde{C}_{ijkl}} \cdot \boldsymbol{\kappa}^{-1} = -\boldsymbol{\kappa}^{-1} \cdot \left(\boldsymbol{\xi} \cdot \frac{\partial \tilde{\mathbf{C}}}{\partial \tilde{C}_{ijkl}} \cdot \boldsymbol{\xi} \right) \boldsymbol{\kappa}^{-1}. \tag{A.9}$$

Taking into account the symmetries of the effective elastic moduli tensor, its derivatives read

$$\begin{aligned}
\frac{\partial \tilde{C}_{mnpq}}{\partial \tilde{C}_{ijkl}} &= \frac{1}{8} (\delta_{mi}\delta_{nj}\delta_{pk}\delta_{ql} + \delta_{ni}\delta_{mj}\delta_{pk}\delta_{ql} + \delta_{mi}\delta_{nj}\delta_{qk}\delta_{pl} + \delta_{ni}\delta_{mj}\delta_{qk}\delta_{pl} + \\
&\quad \delta_{pi}\delta_{qj}\delta_{mk}\delta_{nl} + \delta_{qi}\delta_{pj}\delta_{mk}\delta_{nl} + \delta_{pi}\delta_{qj}\delta_{nk}\delta_{ml} + \delta_{qi}\delta_{pj}\delta_{nk}\delta_{ml}).
\end{aligned}$$

454 The Hill tensor and its partial derivatives have been computed numerically
455 using Gauss quadrature.

456 **B Details on the full-field FFT implementation**

457 The FFT full-field modelling has been implemented using the original scheme
458 of Moulinec and Suquet (1998) since the studied material (i.e. an elastic poly-
459 crystal) presents a moderate contrast in local mechanical properties. Concern-
460 ing numerical aspects, use has been made of the FFTW package (<http://www.fftw.org>)
461 developed by Frigo and Johnson (2005). The computations have been per-
462 formed on a mono-processor computer (2.33GHz). The efficiency of our imple-
463 mentation has been tested for the same polycrystalline unit cell with different
464 discretization grids. The discretization of the unit cell ranges from $N = 16^3$
465 to $N = 320^3$. The CPU time per elastic iteration is reported in Figure 8. As
466 expected, the computing time scales linearly with $N \log N$. It is noted that
467 the chosen FFT package allows to get approximately the same scaling even
468 when the number of voxels along each direction ($\sqrt[3]{N}$) is a prime number. For
469 a local elastic anisotropy parameter $A = 2.8$, five FFT iterations are required
470 in average to solve the problem with a relative error of 10^{-6} on the stress equi-
471 librium condition. It is also interesting to consider the efficiency of the method
472 in terms of memory size requirements. The size of a problem is characterized
473 by the number of d.o.f. which is equal to $3N$. For illustration, the amount of
474 memory required by our implementation of the full-field FFT modelling for
475 $\sqrt[3]{N} = 128$ (~ 6 millions d.o.f) is 1 gigabyte (compare with a recent study
476 using FEM that required 21 gigabytes of memory to solve a similar problem
477 with less than 1 million d.o.f (Houdaigui et al., 2007)).

478 **References**

- 479 Bergman, D. J., 1978. The dielectric constant of a composite material – a
480 problem in classical physics. *Physics Reports* 43, 377–407.
- 481 Bobeth, M., Diener, G., 1987. Static and thermoelastic field fluctuations in
482 multiphase composites. *J. Mech. Phys. Solids* 35, 137–149.
- 483 Brenner, R., Castelnau, O., Badaea, L., 2004. Mechanical field fluctuations in
484 polycrystals estimated by homogenization techniques. *Proc. R. Soc. Lond.*
485 A460, 3589–3612.
- 486 Budiansky, B., Hashin, Z., Sanders, J. L., 1960. The stress field of a slipped
487 crystal and the early plastic behavior of polycrystalline materials. In: *Plas-*
488 *ticity*, Proc. 2nd Symp. Naval Struct. Mech. Pergamon, Oxford, p. 239.
- 489 Castelnau, O., Blackman, D. K., Lebensohn, R. A., Ponte Castañeda, P., 2008.

- 490 Micromechanical modeling of the viscoplastic behavior of olivine. *J. Geophys. Res.* 113, B09202.
- 491
- 492 Castelnau, O., Brenner, R., Lebensohn, R. A., 2006a. The effect of strain
493 heterogeneity on the work hardening of polycrystals predicted by mean-
494 field approaches. *Acta Mater.* 54, 2745–2756.
- 495 Castelnau, O., Goudeau, P., Geandier, G., Tamura, N., Béchade, J., Bornert,
496 M., Caldemaison, D., 2006b. White beam microdiffraction experiments for
497 the determination of the local plastic behaviour of polycrystals. *Mater. Sci.*
498 *Forum* 524–525, 103–108.
- 499 Clausen, B., Lorentzen, T., Leffers, T., 1998. Self-consistent modelling of the
500 plastic deformation of fcc polycrystals and its implications for diffraction
501 measurements of internal stresses. *Acta mater.* 46, 3087–3098.
- 502 Eshelby, J. D., 1957. The determination of the elastic field of an ellipsoidal
503 inclusion, and related problems. *Proc. R. Soc. Lond.* A241, 376–396.
- 504 Eyre, D. J., Milton, G. W., 1999. A fast numerical scheme for computing the
505 response of composites using grid refinement. *Journal of Physique III* 6,
506 41–47.
- 507 Frigo, M., Johnson, S. G., 2005. The design and implementation of FFTW3.
508 *Proceedings of the IEEE* 93 (2), 216–231, special issue on "Program Gen-
509 eration, Optimization, and Platform Adaptation".
- 510 Geandier, G., Gélébart, L., Castelnau, O., Bourhis, E. L., Renault, P.-O.,
511 Goudeau, P., Thiaudière, D., 2008. *IUTAM Book Series*. Springer, Ch. Mi-
512 cromechanical modeling of the Elastic Behavior of Multilayer Thin Films;
513 Comparison with in situ data from X-Ray Diffraction.
- 514 Hashimoto, K., Margolin, H., 1983a. The role of elastic interaction stresses on
515 the onset of slip in polycrystalline alpha brass – I. experimental determi-
516 nation of operating slip systems and qualitative analysis. *Acta Metall.* 31,
517 773–785.
- 518 Hashimoto, K., Margolin, H., 1983b. The role of elastic interaction stresses on
519 the onset of slip in polycrystalline alpha brass – II. rationalization of slip
520 behavior. *Acta Metall.* 31, 786–800.
- 521 Hershey, A. V., 1954. The elasticity of an isotropic aggregate of anisotropic
522 cubic crystals. *J. Appl. Mech.* 21, 236–240.
- 523 Hill, R., 1952. The elastic behaviour of a crystalline aggregate. *Proc. Phys.*
524 *Soc.* A65, 349–354.
- 525 Hill, R., 1963. Elastic properties of reinforced solids : some theoretical princi-
526 ples. *J. Mech. Phys. Solids* 11, 357–372.
- 527 Hill, R., 1967. The essential structure of constitutive laws for metal composites
528 and polycrystals. *J. Mech. Phys. Solids* 15, 79–95.
- 529 Hook, R. E., Hirth, J., 1967. The deformation behavior of isoaxial bicrystals
530 of fe-3%Si. *Acta Metall.* 15, 535–551.
- 531 Houdaigui, F. E., Forest, S., Gourgues, A.-F., Jeulin, D., 2007. On the size
532 of the representative volume element for isotropic elastic polycrystalline
533 copper. In: Bai, Y. (Ed.), *IUTAM Symposium on Mechanical Behavior and*
534 *Micro-Mechanics of Nanostructured Materials*. pp. 171–180.

- 535 Hutchinson, J. W., 1970. Elastic-plastic behaviour of polycrystalline metals
536 and composites. *Proc. R. Soc. Lond.* A319, 247–272.
- 537 Kreher, W., 1990. Residual stresses and stored elastic energy of composites
538 and polycrystals. *J. Mech. Phys. Solids* 38, 115–128.
- 539 Kröner, E., 1958. Berechnung der elastischen konstanten des vielkristalls aus
540 den konstanten des einkristalls. *Z. Physik* 151, 504–518.
- 541 Kröner, E., 1961. Zur plastischen verformung des vielkristalls. *Acta Metall.*
542 *Mater.* 9, 155–191.
- 543 Kröner, E., 1977. Bounds for effective elastic moduli of disordered materials.
544 *J. Mech. Phys. Solids* 25, 137–156.
- 545 Kröner, E., 1978. Self-consistent scheme and graded disorder in polycrystal
546 elasticity. *J. Phys. F: Metal Phys.* 8, 2261–2267.
- 547 Kumar, S., Kurtz, S. K., 1994. Simulation of material microstructure using a
548 3d voronoi tessellation: calculation of effective thermal expansion coefficient
549 of polycrystalline materials. *Acta Metall. Mater.* 42, 3917–3927.
- 550 Kumar, S., Kurtz, S. K., Agarwala, V. K., 1996. Micro-stress distribution
551 within polycrystalline aggregate. *Acta Mechanica* 114, 203–216.
- 552 Lebensohn, R. A., 2001. N-site modeling of a 3D viscoplastic polycrystal using
553 fast fourier transform. *Acta Mater.* 49, 2723–2737.
- 554 Lebensohn, R. A., Liu, Y., Ponte Castañeda, P. , 2004. On the accuracy of
555 the self-consistent approximation for polycrystals: comparison with full-field
556 numerical simulations. *Acta Materialia* 52, 5347–5361.
- 557 Margolin, H., Wang, Z., Chen, T.-K., 1986. A model for yielding in anisotropic
558 metals. *Metallurgical Transactions A* 17A, 107–114.
- 559 Mehrabadi, M. M., Cowin, S. C., 1990. Eigentensors of linear anisotropic elas-
560 tic materials. *Quart. J. Mech. Appl. Math.* 43, 15–41.
- 561 Mendelson, K. S., 1981. Bulk modulus of a polycrystal. *J. Phys. D: Appl.*
562 *Phys.* 14, 1307–1309.
- 563 Meyers, M. A., Ashworth, E., 1982. A model for the effect of grain size on the
564 yield stress of metals. *Philosophical Magazine A* 46, 737–759.
- 565 Michel, J. C., Moulinec, H., Suquet, P., 2001. A computational scheme for lin-
566 ear and non-linear composites with arbitrary phase contrast. *Int. J. Numer.*
567 *Meth. Engng* 52, 139–160.
- 568 Moulinec, H., Suquet, P., 1998. A numerical method for computing the overall
569 response of nonlinear composites with complex microstructure. *Comput.*
570 *Methods Appl. Mech. Engrg.* 157, 69–94.
- 571 Moulinec, H., Suquet, P., 2003. Intraphase strain heterogeneity in nonlinear
572 composites: a computational approach. *Eur. J. Mech. A/Solids* 22, 751–770.
- 573 Nygards, M., 2003. Number of grains necessary to homogenize elastic materials
574 with cubic symmetry. *Mech. Mater.* 35, 1049–1057.
- 575 Nygards, M., Gudmundson, P., 2002. Three-dimensional periodic voronoi grain
576 models and micromechanical fe-simulations of a two-phase steel. *Computa-*
577 *tional Materials Science* 24, 513–519.
- 578 Pang, J., Holden, T., Turner, P., Mason, T., 1999. Intergranular stresses in
579 zircaloy-2 with rod texture. *Acta Mater.* 47 (2), 373–383.

- 580 Ponte Castañeda, P., Suquet, P., 1998. Nonlinear composites. *Adv. Appl.*
581 *Mech.* 34, 171–302.
- 582 Sab, K., 1992. On the homogenization and the simulation of random materials.
583 *Eur. J. Mech. A/Solids* 11, 585–607.
- 584 Sauzay, M., 2007. Cubic elasticity and stress distribution at the free surface
585 of polycrystals. *Acta Mater.* 55, 1193–1202.
- 586 Tamura, N., MacDowell, A., Spolenak, R., Valek, B., Bravman, J., Brown,
587 W., Celestre, R., Padmore, H., Batterman, B., Patel, J., 2003. Scanning x-
588 ray microdiffraction with submicrometer white beam for strain/stress and
589 orientation mapping in thin films. *J. Synch. Rad.* 10, 137–143.
- 590 Turner, P. A., Christodoulou, N., Tomé, C. N., 1995. Modeling the mechanical
591 response of rolled zircaloy-2. *Int. J. Plasticity* 11, 251–265.
- 592 Ungár, T., Castelnau, O., Ribárik, G., Drakopoulos, M., Béchade, J., Chau-
593 veau, T., Snigirev, A., Snigireva, I., Schroer, C., Bacroix, B., 2007. Grain
594 to grain slip activity in plastically deformed zr determined by x-ray micro-
595 diffraction line profile analysis. *Acta Mater.* 55, 1117–1127.
- 596 Wikström, A., Nygards, M., 2002. Anisotropy and texture in thin copper films
597 : an elastoplastic analysis. *Acta Mater.* 50, 857–870.
- 598 Willis, J. R., 1977. Bounds and self-consistent estimates for the overall prop-
599 erties of anisotropic composites. *J. Mech. Phys. Solids* 25, 185–202.
- 600 Yaguchi, M., Busso, E. P., 2005. On the accuracy of self-consistent elasticity
601 formulations for directionally solidified polycrystal aggregates. *Int. J. Solids*
602 *Struct.* 42, 1073–1089.
- 603 Zeghadi, A., N’Guyen, F., Forest, S., Gourgues, A.-F., Bouaziz, O., 2007.
604 Ensemble averaging stress-strain fields in polycrystalline aggregates with a
605 constrained surface microstructure - part 1: anisotropic elastic behaviour.
606 *Phil. Mag. A* 87, 1401–424.
- 607 Zeller, R., Dederichs, P. H., 1973. Elastic constants of polycrystals. *Phys.*
608 *Status Solidi (b)* 55, 831–842.
- 609 Zener, C., 1948. *Elasticity and anelasticity of Metals*. University Chicago
610 Press.

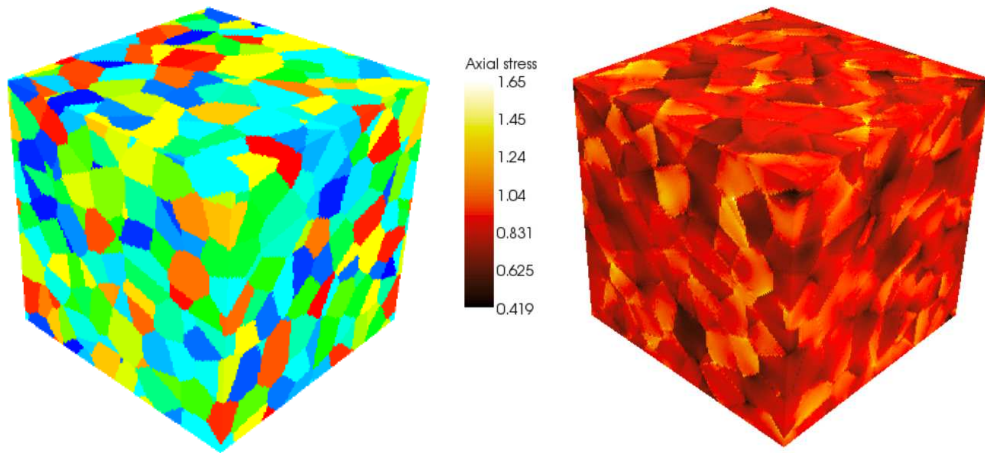


Fig. 1. Periodic Poisson-Voronoi tessellation containing 500 grains with uniform crystalline orientations (a) and corresponding axial stress field for a tensile loading (b)

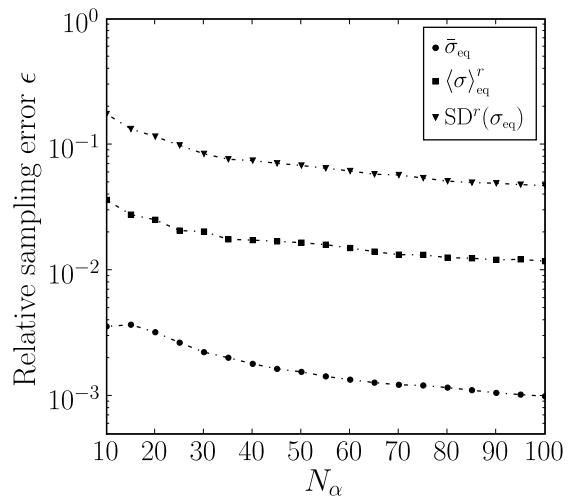


Fig. 2. Relative sampling error of the stress field at different scales vs. the number of unit-cell realizations

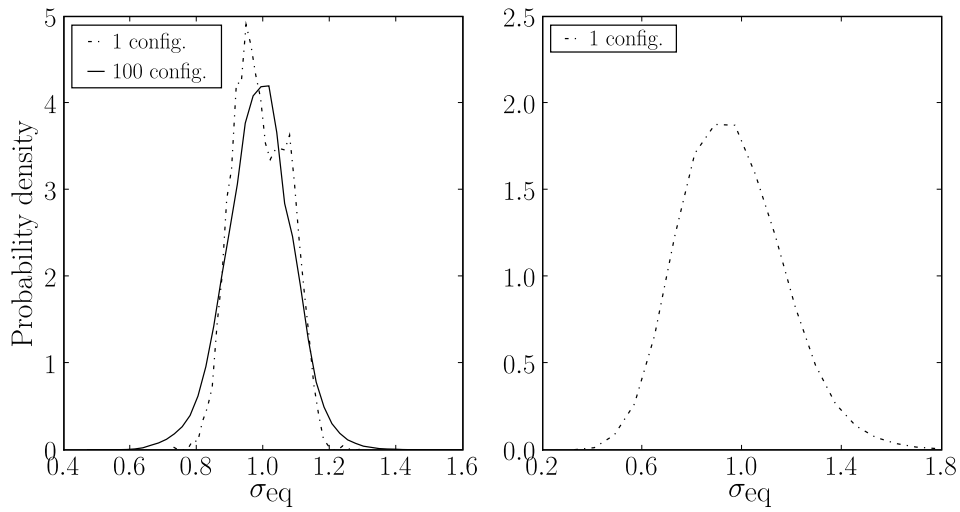


Fig. 3. Normalized equivalent stress field distribution within a single crystalline orientation (left) and within the whole unit-cell (right). Note that a similar distribution is obtained with 100 configurations for the whole unit-cell.

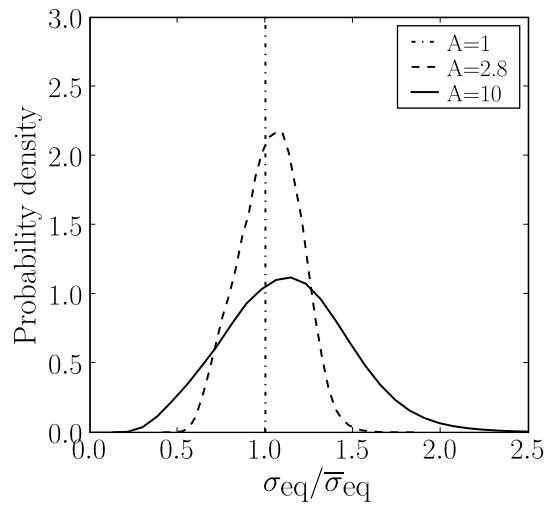


Fig. 4. Distribution of the equivalent stress field distribution within a polycrystalline RVE, for different values of the Zener parameter A , as obtained by the full-field approach.

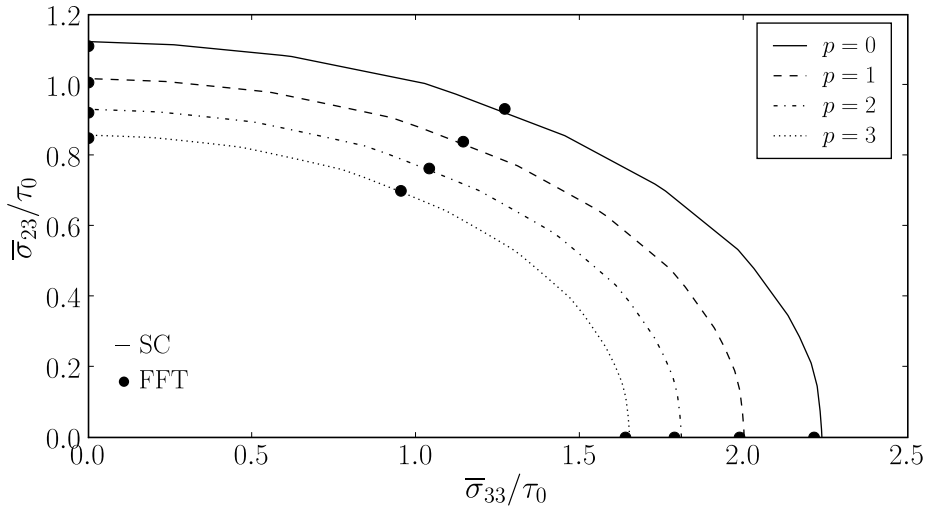


Fig. 5. Self-consistent estimates of yield surface sections obtained with different p values for tension-torsion loadings (curves). FFT estimates are reported for three different loading paths (symbols)

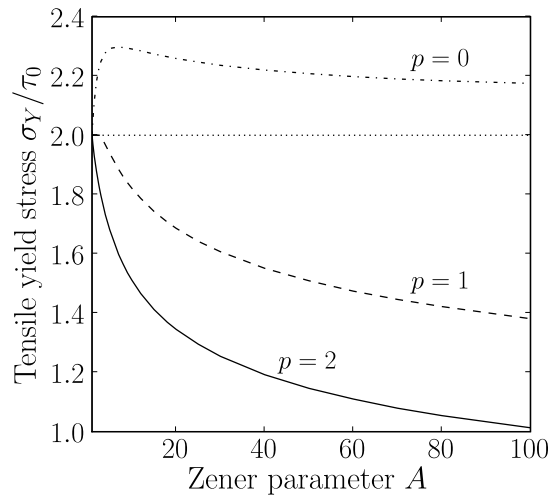


Fig. 6. Self-consistent estimates of the tensile yield stress as a function of the Zener parameter A . Note that the case $p = 0$ corresponds to Hutchinson's estimate. The horizontal dotted line indicates the value of the Tresca yield stress.

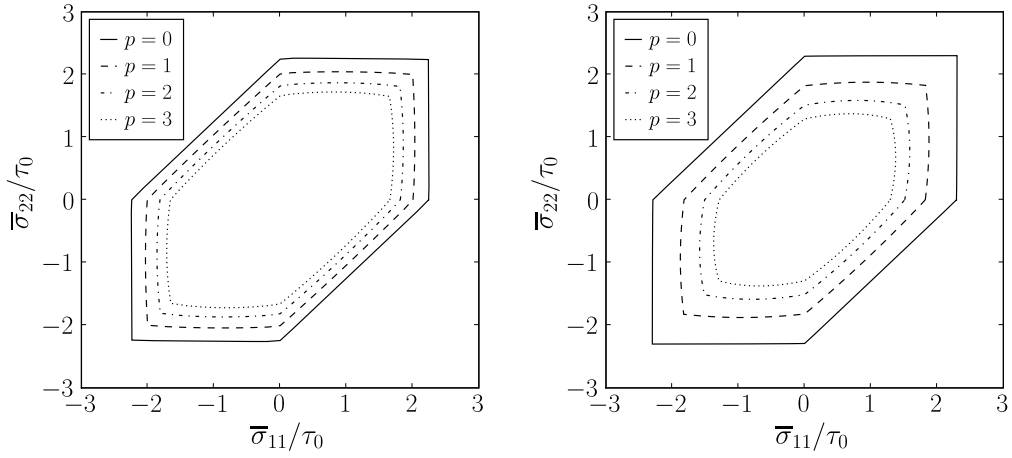


Fig. 7. Self-consistent estimates of yield surface sections obtained with different p values for biaxial loadings. $A = 2.8$ (left) and $A = 10$ (right).

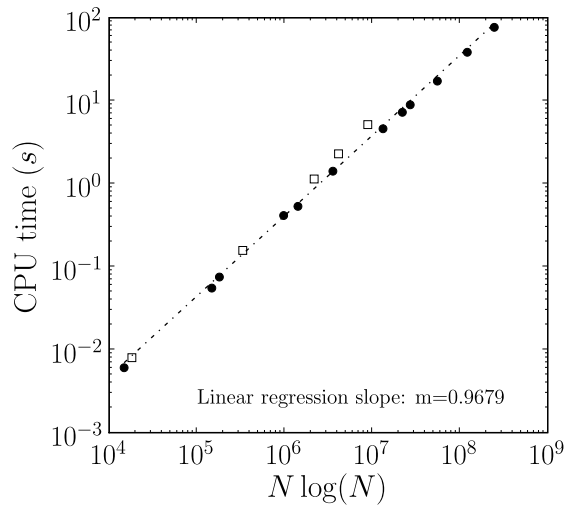


Fig. 8. CPU time per elastic FFT iteration as a function of the number of voxels N . The white squares correspond to unit-cell discretizations with prime numbers in each direction.